Supporting Information

Unveiling the role of local temperature gradients in individual zeolites containing metal active sites

B*ing Zhao[a,b], Zhikang Xu[e], Guida Li[a,b], Gang Meng[a], Hang Chen[b], Tong Zhao[f], Haibo Zhu[d], Dan Zhao[b], Mingbin Gao[c,*], Mao Ye[a,b,*] and Zhongmin Liu[b]*

[a]Department of Chemical Physics, University of Science and Technology of China, Hefei, Anhui, China, 230026

[b]Dalian Institute of Chemical Physics, Chinese Academy of Sciences, Dalian, Liaoning, China, 116023

[c]Department of Chemical and Biochemical Engineering, College of Chemistry and Chemical Engineering, State Key Laboratory of Physical Chemistry of Solid Surfaces, Xiamen University, Xiamen, Fujian, China, 361005

[d]National Engineering Research Center of Chemical Fertilizer Catalyst, School of Chemical Engineering, Fuzhou University, Fuzhou, Fujian, China, 350002

[e]Qingyuan Innovation Laboratory, Quanzhou, China, 362801

[f]Analytical Solution Plaza, HORIBA (China) Trading Co., Shanghai, China, 200335

*: corresponding author:

E-mail addresses: mbgao@xmu.edu.cn (Mingbin Gao); maoye@dicp.ac.cn (Mao Ye)

Table of Contents

1. Experiments

1.1 Catalyst preparation

Preparation of large-sized S-1 zeolite. The large-sized S-1 zeolite (the length of *c*-axis of zeolite, L_c=120 μm) was prepared via a hydrothermal crystallization method. In a typical procedure, 16.48 g of tetraethyl orthosilicate (TEOS), 16.24 g of tetrapropyl ammonium hydroxide (TPAOH), and 16.88 g of deionized water were mixed in a beaker and stirred continuously for 4 hours at room temperature. Subsequently, 4.00 g of ammonium fluoride (NH_4F) was gradually introduced into the mixture while stirring vigorously. The resulting homogeneous mixture was transferred into a 100 ml Teflon-lined stainless-steel autoclave and subjected to hydrothermal treatment at 170 °C for 72 hours under static conditions. After cooling to room temperature, the crystalline product was collected by filtration, thoroughly washed with deionized water until the filtrate reached neutral pH, and dried at 120 °C for 12 hours. Finally, the large-sized S-1 zeolite (L_c=120 μm) was obtained by calcining the dried precursor at 550 °C for 6 hours.

Preparation of 5% CoO_x@S-1-M catalyst. The 5 wt% CoO_x@S-1-M catalyst was synthesized via a conventional wet impregnation method. Specifically, 0.25 g of cobalt(II) nitrate hexahydrate ($Co(NO_3)_2·6H_2O$) was dissolved in 1.00 g of deionized water to prepare a homogeneous precursor solution. This solution was thoroughly mixed with 1.00 g of large-crystal S-1 zeolite and allowed to stand at room temperature for 12 h. The resulting material was then dried at 120 °C for 12 h, followed by calcination at 550 °C for 6 h to obtain the final catalyst.

Preparation of 5% CoO_x@S-1-U catalyst. The 5 wt% CoO_x@S-1-U catalyst was synthesized using an ultrasound-assisted impregnation method. In a typical procedure, 0.25 g of cobalt(II) nitrate hexahydrate ($Co(NO_3)_2·6H_2O$) was dissolved in 1.00 g of deionized water to prepare a homogeneous precursor solution. This solution was mixed with 1.00 g of large-crystal S-1 zeolite, followed by ultrasonic treatment for 12 h to promote uniform dispersion of cobalt species within the zeolite framework. The resulting material was then dried at 120 °C for 12 h and calcined at 550 °C for 6 h to yield the final catalyst.

Tetraethylorthosilicate (TEOS, 99.99%); Tetrapropylammonium hydroxide solution (TPAOH, 40%); Cobalt nitrate hexahydrate ($Co(NO_3)_2 \cdot 6H_2O$, 99.9%); Ammonium fluoride (NH_4F, 96%). Deionized water was obtained from a water purification system with a resistivity of 18.2 $M\Omega \cdot cm^{-1}$. The chemicals mentioned above were used directly without undergoing any further processing.

1.2 Characterizations

X-ray powder diffraction (XRD). The phase analysis of the molecular sieve sample was conducted using an X-ray powder diffractometer (PANalytical X'Pert PRO, Netherlands). The analysis was performed with a copper target and Kα radiation source (λ = 0.154059 nm), operating at a tube voltage of 40 kV and a current of 40 mA. The scanning range was set from 5° to 60°, with a scanning speed of 5 °/min.

Magic-Angle Spinning Nuclear Magnetic Resonance (MAS NMR). ^{29}Si MAS NMR was performed on BRUKER AVANCE III HD 400MHz (WB) and were carried out on a Varian 400 MHz spectrometer equipped with a wideband probe in $\lambda/2$ mode. The spectra were recorded under magic-angle spinning conditions with a spectral width (SWH) of 25,000 Hz. Each spectrum was acquired with 1024 scans (*ns* = 1024) and a recycle delay of 10 s (d1 = 10 s).

Inductively Coupled Plasma Optical Emission Spectrometry (ICP-OES). ICP-OES was performed on PerkinElmer Avio 550 Max.

Nitrogen physical adsorption. The surface area and pore volume of the molecular sieve samples were determined using a Micromeritics ASAP 2020 physisorption instrument (USA). Initially, the samples were heated to 623 K under vacuum at room temperature, followed by a dehydration treatment at 623 K for 240 minutes. The free volume within the sample tube was measured using helium as the medium. For the analysis, nitrogen was used as the adsorbate at liquid nitrogen temperature (77 K) to conduct isothermal adsorption and desorption measurements. The surface area was calculated using the BET method, while the total pore volume was determined from the nitrogen adsorption at a relative pressure (P/P_0) of 0.99. The micropore surface area

and volume were estimated using the t-plot method, with the cross-sectional area of nitrogen molecules set at 0.162 nm^2.

X-ray absorption spectroscopy (XAS). Co K-edge (7709 eV) X-ray absorption spectroscopy (XAS) in transmission mode was performed using a Rapid XAFS 2M system, operating at 20 kV and 40 mA. A Si (533) spherical crystal analyzer with a curvature radius of 500 mm was employed, and foil and Co_2O_3 were used as reference samples. The data collected in the k-space range of 0 to 8 $Å^{-1}$ were Fourier transformed into real (R) space using a Hanning window (dk = 1.0 $Å^{-1}$), which enabled the isolation of EXAFS contributions from different coordination shells.

Time-of-Flight Secondary Ion Mass Spectrometry (TOF-SIMS). The spatial distribution of Co ions within the molecular sieve crystals was analyzed using time-of-flight secondary ion mass spectrometry (TOF-SIMS) (IONTOF GmbH, M6 model). The samples were mounted with siloxane-free double-sided tape and then placed under vacuum in the instrument. After adjusting the primary ion beam's energy and intensity, the sample surface was bombarded, generating secondary ions. These ions were accelerated into the time-of-flight analyzer, where their mass-to-charge ratio was determined based on the time it took for them to reach the detector. The mass spectrum was analyzed to identify characteristic peaks, and secondary ion images were generated to reveal the spatial distribution of elements or molecules within the samples.

O_2-Temperature Programmed Oxidation (O_2-TPO) experiments. O_2-TPO were conducted to investigate the oxidation behavior of the spent catalysts. Approximately 50 mg of the sample was loaded into a U-shaped quartz reactor and pretreated under an Ar atmosphere (40 mL min^{-1}) by heating to 300 °C and maintaining this temperature for 30 min to remove adsorbed moisture and impurities. After the temperature was decreased to 100 °C and stabilized for 10 min, a mixed gas containing 5 vol% O_2 (balanced with Ar, total flow rate of 10 mL min^{-1}) was introduced. The temperature was then increased from 100 °C to 800 °C at a ramping rate of 10 °C min^{-1} under the 5% O_2/Ar atmosphere. The signals of CO_2 (m/z = 44) and Ar (m/z = 40) were continuously recorded during the oxidation process.

Diffuse Reflectance Ultraviolet-visible (DR UV-vis) spectroscopy measurements. DR UV-vis were carried out on a VARIAN Cary-5000 UV-Vis-NIR spectrophotometer. Approximately 20 mg of the zeolite sample was placed in a crucible and loaded into a PIKE *in situ* reaction cell equipped with a temperature controller and quartz windows. The spectra were recorded in the wavelength range of 200-800 nm with a scanning rate of 10 nm min^{-1}.

Matrix-assisted laser desorption/ionization Fourier transform ion cyclotron resonance mass spectrometry (MALDI FT-ICR MS). Three measurement modes were employed to selectively probe coke species located on the external surface, in the organic extract, and within the insoluble residue, respectively. All spectra were acquired in the positive ion mode under identical instrumental settings. Mode I: Analysis of surface coke species. Purpose: To detect coke species located on the external surface of the spent zeolite catalyst. A tetrahydrofuran (THF) solution containing 1,8,9-anthracenetriol (MALDI matrix, 5 mg ml^{-1}) was first prepared. Then, 5 mg of the spent catalyst was dispersed in 0.5 mL of the above matrix solution and ultrasonicated to obtain a homogeneous suspension. A 1 μL aliquot of the suspension was dropped onto the MALDI target plate and dried at room temperature. The sample was then introduced into the ionization chamber for analysis using a Nd:YAG laser (λ = 335 nm). The laser repetition rate was set to 200 Hz, and 64 laser shots per spot were accumulated in a random-walk mode. The mass range was set to $150 < m/z < 1200$, and the instrument was calibrated using a peptide standard mixture before measurement. Mode II: Analysis of organic extract-derived coke species. Purpose: To characterize soluble coke species extracted into the organic phase after catalyst deactivation. In this mode, 10 μL of the organic extract was mixed with 10 μL of the THF solution containing 1,8,9-anthracenetriol (5 mg ml^{-1}). The mixture was ultrasonicated to ensure homogeneous dispersion. Then, 1 μL of the resulting mixture was deposited onto the target plate and dried under ambient conditions. The prepared target was analyzed under the same MALDI FT-ICR MS conditions as described for the spent catalyst to enable direct comparison of coke species in different environments. Mode III: Analysis of insoluble

coke species. Purpose: To examine the structure of the insoluble, polymeric coke residues separated from the spent catalyst. Approximately 1 mg of the collected insoluble coke powder was suspended in 200 μL of THF containing 1,8,9-anthracenetriol (5 mg ml^{-1}). The suspension was ultrasonicated to obtain a uniform dispersion, and 1 μL of the resulting mixture was spotted onto the target plate. After drying at room temperature, the sample was analyzed under the same MALDI FT-ICR MS conditions as in the previous modes.

Kendrick mass defect (KMD) analysis was employed to identify homologous series in the mass spectra. The Kendrick mass (KM) was calculated as KM = ObservedMass × (14.00000/14.01565) for CH_2 as the repeat unit, and the Kendrick mass defect (KMD) was defined as KMD = round(KM) − KM. Peaks with identical KMD values (within ±0.001) and with m/z differences close to 14.01565 u were assigned to the same CH_2-homologous family. Representative peaks were validated by MS/MS fragmentation and labeled with consistent colors in both the original mass spectrum and the KMD plot.

X-ray Photoelectron Spectroscopy (XPS). The surface chemical states of the samples were analyzed by XPS using a Thermo Scientific ESCALAB 250Xi spectrometer equipped with a monochromatic Al Kα radiation source (hν = 1486.6 eV). The samples were thoroughly dried prior to measurement and analyzed under ultra-high vacuum conditions (~10^{-9} mbar). All binding energies were calibrated with respect to the C 1s peak at 284.8 eV.

Intelligent Gravimetric Analyzer (IGA). The dynamic adsorption curves and isothermal adsorption isotherms of propane on the molecular sieve were measured using a Hiden Analytical intelligent gravimetric analyzer (UK). To enhance the interaction between the gas and the sample, a custom-designed mesh sample holder was employed, replacing the instrument's standard quartz holder. Typically, 20-30 mg of the molecular sieve (40-60 mesh, with catalyst mass adjusted depending on the system) was placed in the sample holder. The chamber was initially evacuated to 10^{-6} mbar, then heated to 623 K and maintained at this temperature for 240 minutes. The sample's weight change was continuously monitored, and dehydration was considered complete

when the weight stabilized. Following this, the sample holder temperature was reduced to 25 °C, and a non-flowing gas at a specified pressure was introduced for the dynamic adsorption experiment. During the adsorption process, the sample's weight increased (corrected for buoyancy), and this dynamic process was recorded until equilibrium was reached, indicating that the gas had saturated the sample at the given pressure. Both the pressure and temperature within the sample holder were continuously monitored. Prior to experimentation, the molecular sieve sample mass was adjusted to ensure that it did not affect the dynamic adsorption curve, thus eliminating any potential influence from external gas diffusion effects. Furthermore, using a smaller sample mass helped minimize thermal effects induced by adsorption heat. Finally, isothermal adsorption curves were generated by measuring the saturation adsorption of gas at 25 °C, 40 °C, and 55 °C, 70 °C across a pressure range of 0-10 mbar.

The surface permeability can be firstly determined by the model

$$\frac{m_t}{m_\infty}|^{\sqrt{t}\to 0} \cong \frac{\alpha}{l}\left(\sqrt{t}\right)^2 \qquad S1$$

via initial uptake curves (quadratic function form) in Fig. S7, (m_t/m_∞ is the relative uptake loading of guest molecules. t is the uptake time. l is the half thickness of the plane sheet, *i.e*. half L_b of S-1 sample. α is the surface permeability.) With the value of surface permeability determined from Equation S1, the inverse of diffusion time constant D/l^2 can be obtained by fitting the whole uptake curve through Equation S2.

The relative uptake loading mt/m∞ of guest molecules in a plane sheet can be described by the dual resistance model (DRM). Fitting the whole uptake curve in Fig. S7 can obtain the D/l^2

$$\frac{m_t}{m_\infty} == 1 - \sum_{n=1}^{\infty} \frac{2L^2 \exp\left(-\frac{\beta_n^2 Dt}{l^2}\right)}{(\beta_n^2 + L^2 + L)\beta_n^2}; \beta_n tan\beta_n = L \qquad S2$$

D is the intracrystalline (transport) diffusivity. $L = \alpha l/D$ is the ratio of characteristic time of intracrystalline diffusion to that of surface barriers. The DRM model used to fit the experimental uptake data was coded by the MATLAB software, the 'fminsearch' was employed as the fitting function in the MATLAB. The detailed fitting results of the

inverse of diffusion and surface permeation time constant by Equations S1 and S2 are shown in Supplementary Tables 4 and 5.

1.3 *In situ* Raman thermometry. Raman spectra were collected using a Horiba LabRAM Odyssey spectrometer (spectral resolution: 0.34 cm^{-1}) with a 532 nm excitation laser. The Raman measurements were performed using a confocal microscopic configuration, in which out-of-focus scattering signals were suppressed by the pinhole in the excitation and collection paths. The focal plane was adjusted by moving the sample along the Z axis, allowing Raman signals to be collected from a defined depth within the crystal. Under the present conditions, the typical focusing depth was approximately 7 μm, corresponding to about half of the crystal thickness, indicating that the collected Raman signal was not limited to the external surface but originated from the crystal interior. Measurement parameters were set to 10% laser power, a 20 s exposure time, and a single accumulation per spectrum. *In situ* Raman experiments were performed using a Linkam CCR1000 reaction cell mounted beneath the microscope objective. The cell was connected to gas lines for propane, hydrogen, nitrogen, and air, with flow rates regulated by mass flow controllers and valves. The catalyst was initially pretreated in H_2. After H_2 was discontinued, N_2 was introduced at 5 $mL \cdot min^{-1}$. The target region of the crystal grain was identified under bright-field illumination, and the laser was focused for spectral acquisition. Temperature was controlled precisely using the reaction cell's integrated system, and Raman spectra were recorded at 5 °C intervals. Upon reaching 575 °C, the system was stabilized before switching to a C_3H_8/N_2 (5 $mL \cdot min^{-1}$) gas mixture to initiate propane dehydrogenation (PDH). Spectra were collected continuously over 30 minutes. After the reaction, propane was stopped, and the system was purged with N_2. Catalyst regeneration was performed under air flow, followed by reintroduction of N_2. The laser was then refocused on a new region of the same crystal grain, and the entire procedure was repeated for additional measurements.

1.4 *In Situ* FT-mIR experiments.

Infrared measurements were conducted using a Bruker Hyperion 3000 confocal infrared microscope at the Shanghai Synchrotron Radiation Facility (Beamline 06B). Spectra were acquired in HYPER10N 3000-MCT-SR-TRANS mode with 400 scans per spectrum and a total acquisition time of 32 seconds. The spectral range covered 600–4000 cm^{-1}. *In situ* infrared experiments were performed using a reaction cell positioned directly beneath the microscope objective. The experimental conditions were consistent with those employed in the *in situ* Raman spectroscopy measurements.

1.5 PL imaging.

Coke species formed via carbon deposition were characterized using a HORIBA LabRAM Odyssey high-speed, high-resolution micro-Raman spectrometer. Measurements were performed with a 40× NUV objective lens under 325 nm excitation, at 1% laser power and a 1-second acquisition time. The spectral range spanned 327-900 nm. PL spectra were collected at 0.6 μm intervals in both the x- and y-directions, from the surface to the interior of individual crystal grains, enabling analysis of both surface and bulk characteristics.

1.6 Propane dehydrogenation experiments

The PDH reaction was carried out in a laboratory-scale fixed-bed reactor system, consisting of four main components: the feed system, vaporization tube, fixed-bed reactor, and gas-phase component analysis system. The feed system includes both gas and liquid feed lines, with the gas flow rate controlled by a mass flow controller. The fixed-bed reactor, made of a quartz tube with an inner diameter of 4 mm, is packed with quartz wool and a specified mass of molecular sieve catalyst. This reactor is placed within an electric heating furnace, ensuring the catalyst is positioned in the isothermal zone of the furnace, where temperature variation remains within ±1 K to minimize experimental error. The product gas exiting the reactor is divided and analyzed quantitatively using an Agilent 7890B gas chromatograph.

Prior to use, the molecular sieve catalyst is calcined to remove organic templates. A 50 mg sample is then loaded into the reactor tube. The catalyst undergoes pretreatment in an H_2 atmosphere (10 mL/min), heated from room temperature to 550 °C at a rate of

5 °C/min, and held at this temperature for 1 hour. After pretreatment, propane (20% diluted with nitrogen) is introduced into the reactor at a space velocity of 1.92 $mL \cdot g^{-1} \cdot min^{-1}$, with the reactor temperature set to 575°C. The products are analyzed by gas chromatography, using a PoraPLOT Q-HT column and a flame ionization detector (FID). Kinetic data for the PDH reaction are obtained by varying the reaction temperature.

Catalytic performance calculations: The molar flow rates of H_2, CH_4, C_2H_4, C_2H_6, C_3H_6 and C_3H_8 in outlet were measured and calculated by using He as a reference gas. The He was introduced into the outlet of the PDH reactor as a reference gas. The product mixture was analyzed by GC. The He was detected by TCD detector, and CH_4, C_2H_4, C_2H_6, C_3H_6 and C_3H_8 were detected by FID detector.

Propane conversion, propylene selectivity and carbon balance (> 98%) were calculated on the carbon basis by Equations S3 to S5, respectively.

$$\text{Propane conversion (\%)} = \frac{\left[F_{C_3H_8}\right]_{\text{inlet}} - \left[F_{C_3H_8}\right]_{\text{outlet}}}{\left[F_{C_3H_8}\right]_{\text{inlet}}} \times 100\% \qquad \text{S3}$$

$$\text{Propane selectivity (\%)} = \frac{\left[F_{C_3H_6}\right]_{\text{outlet}}}{\left[F_{C_3H_8}\right]_{\text{inlet}} - \left[F_{C_3H_8}\right]_{\text{outlet}}} \times 100\% \qquad \text{S4}$$

$$\text{Carbon balance (\%)} = \frac{\frac{1}{3}\left[F_{CH_4}\right]_{\text{outlet}} + \frac{2}{3}\left[F_{C_2H_6}\right]_{\text{outlet}} + \frac{2}{3}\left[F_{C_2H_4}\right]_{\text{outlet}} + \left[F_{C_3H_6}\right]_{\text{outlet}} + \left[F_{C_3H_8}\right]_{\text{outlet}}}{\left[F_{C_3H_8}\right]_{\text{inlet}}} \times 100\% \qquad \text{S5}$$

Inactivation constant:

$$k_d t = \ln\left(\frac{1 - X_{final}}{X_{final}}\right) - \ln\left(\frac{1 - X_{initial}}{X_{initial}}\right) \qquad \text{S3}$$

where $X_{initial}$ and X_{final} represent the conversion of C_3H_8 measured at an experiment's initial and final period, t represents the reaction time (h), and k_d is the deactivation rate constant (h^{-1}). A high k_d value means rapid deactivation, that is, low stability.

Catalyst Regeneration: Following the propane dehydrogenation reaction, the system is cooled to below 100 °C. The 20% C_3H_8 valve is closed, and the atmosphere is

switched to air (10 mL/min). In the air atmosphere, the temperature is gradually increased from room temperature to 500 °C at a rate of 5 °C/min, where it is maintained for 2 hours. The system is then cooled, with nitrogen introduced to purge the air from the system during the cooling phase. Once the temperature drops below 100 °C, the air valve is closed, and the atmosphere is switched to hydrogen (H_2) at 10 mL/min for catalyst pretreatment before resuming the propane dehydrogenation reaction.

2. Mass transfer effects

The Mears' and Weisz-Prater' criterions were used to examine the effects of external and internal mass transfer in PDH over CoO_x@S-1-M and CoO_x@S-1-U, respectively.

The external mass transfer effect can be neglected if the following Mears criterion is met.

$$C_M = \frac{-r_A \rho_b R_{cat} n}{k_c C_{Ab}} < 0.15 \qquad S4$$

The internal mass transfer effect can be neglected if the following Weisz-Prater' criterion is met.

$$C_{WP} = \frac{-r_A \rho_c R_{cat}^2}{D_{intra} C_{Ab}} < 1 \qquad S5$$

3. Criterion on internal diffusion limitations (The calculation of Thiele modulus Φ and effectiveness factor η)

The Thiele modulus Φ and effectiveness factor η were used to analyze the effect of internal diffusion constraints of propane in PDH over CoO_x@S-1-M and CoO_x@S-1-U.

Thiele modulus Φ analysis method (reaction order n=1)

$$\Phi = l\sqrt{k/D_{intra}} \qquad S6$$

Effectiveness factor η analysis method ($\Phi < 0.4$)

$$\eta = \frac{\tan\Phi}{\Phi} \qquad S7$$

4. Theoretical simulations

4.1 Periodic ab initio static simulations

Based on the catalyst structure characterizations of CoO_x@S-1, the energy barriers of the elemental steps of activation of propane to propylene and hydrogen catalyzed by Co active species in the MFI framework were performed by periodic DFT. The construction of CoO_x cluster is based on the EXAFS spectra results. Optimizing such structures without any restrictions. All the periodic DFT computations were performed using the plane-wave pseudopotential method and the generalized gradient approximation (GGA), implemented with the CASTEP code. The plane-wave basis set was converged at a cutoff energy of 500 eV for each model. The Perdew-Burke-Ernzerhof (PBE) exchange-correlation function was used to describe the exchange-correlation effects. Interaction between the valence electrons and the ion core was substituted by an ultrasoft pseudopotential. The self-consistent convergence accuracy was set at 2×10^{-5} eV per atom, the maximum force was 0.08 eV per Å, the maximum stress was 0.1 GPa, and the maximum displacement was 5 × 10-3 Å. Here, a single MFI unit cell was employed. A Monkhorst-Pack grid of 1 × 1 × 1 (k-point) was used to sample the Brillouin zone for geometry optimization and for calculating the energy of intermediates. The complete LST/QST method was implemented for transition search of the elemental reaction.

Gibb's free energies (G) can be calculated from DFT-derived energies using statistical mechanics. Specifically, each is a sum of the electronic energy (E), the zero-point vibrational energy (ZPVE), and the corrective free energies Gcorr. at 848 K by thermodynamic correction

$$G = E + ZPVE + G_{\text{corr.}} \qquad S8$$

4.2 Monte Carlo simulations

The spatial probability distribution of propylene within CoO_x@S-1 were obtained from force-filed molecular dynamics (FFMD) simulations. All FFMD simulations in this work were carried out using the Materials Studio package (Acelrys Software). The loading of propylene in CoO_x@S-1 was performed using the grand canonical Monte

Carlo (GCMC) simulation method. The spatial distribution of adsorption probability is counted and visualized. Periodic boundary conditions were applied in all three directions. The interatomic interactions were described by the COMPASS(III) force field, and the electrostatic energy was calculated by the Ewald & Group summation method. The Ewald & Group summation method has an Ewald accuracy of 10^{-5} kcal·mol^{-1} when used for calculating electrostatic potential energy. To achieve an equilibrium state, 107 Monte Carlo steps were carried out.

4.3 Monte Carlo simulations

Self-diffusivities were obtained from molecular dynamics (MD) simulations using the Materials Studio package (Accelrys Software). Molecular adsorption in the MFI framework with CoO_x clusters was modeled by grand canonical Monte Carlo (GCMC) simulations under periodic boundary conditions. The COMPASS force field was applied for interatomic interactions, and electrostatic energies were calculated with the Ewald & Group summation method (accuracy: 10^{-5} kcal·mol^{-1}). To reach equilibrium, 10^7 Monte Carlo steps were performed, considering a flexible zeolite framework and using the Metropolis algorithm at constant temperature and loading. All structures were pre-equilibrated by five annealing cycles between 300 and 900 K. MD simulations were then carried out in the NVT ensemble for 5,000 ps (5,000,000 steps) at 823, 873, 923 and 973 K. The Velocity Verlet algorithm was used with a 1 fs time step, a Lennard–Jones cutoff of 18.5 Å, and temperature control via a Nosé thermostat. The structural models are shown in Supplementary Fig. S10d. Mean square displacements (MSD) of propane are given in Supplementary Fig. S10e, and self-diffusivities were determined from MSD–time slopes according to the Einstein relation.

$$MSD(\tau) = 2nD\tau + b \qquad S9$$

Where n is the dimension of framework (n = 3 for 3D frameworks). b is the thermal factor arising from atomic vibrations.

5. Supplemental Figures

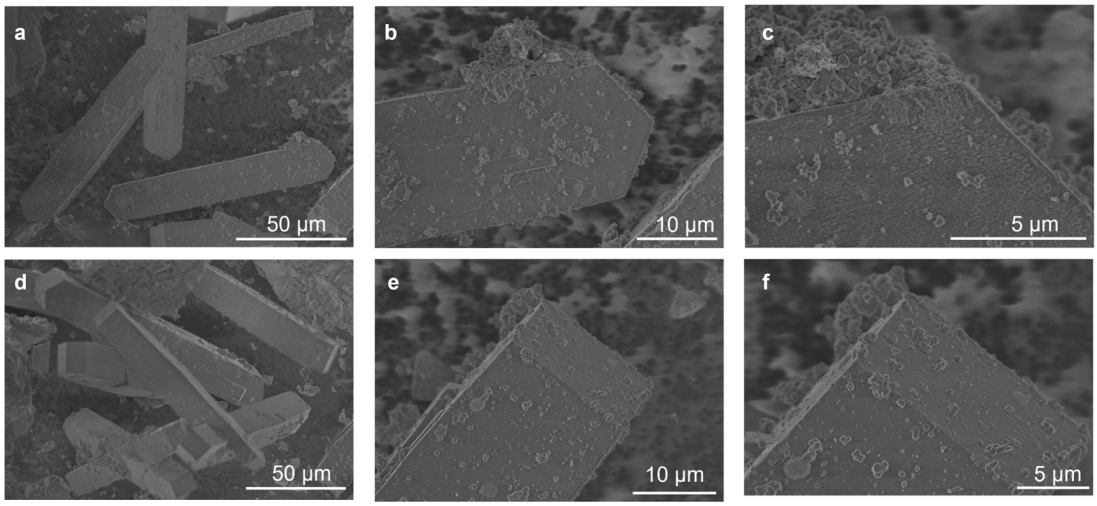

Figure S1. Scanning electron microscopy (SEM) images of CoO_x@S-1-M and CoO_x@S-1-U.

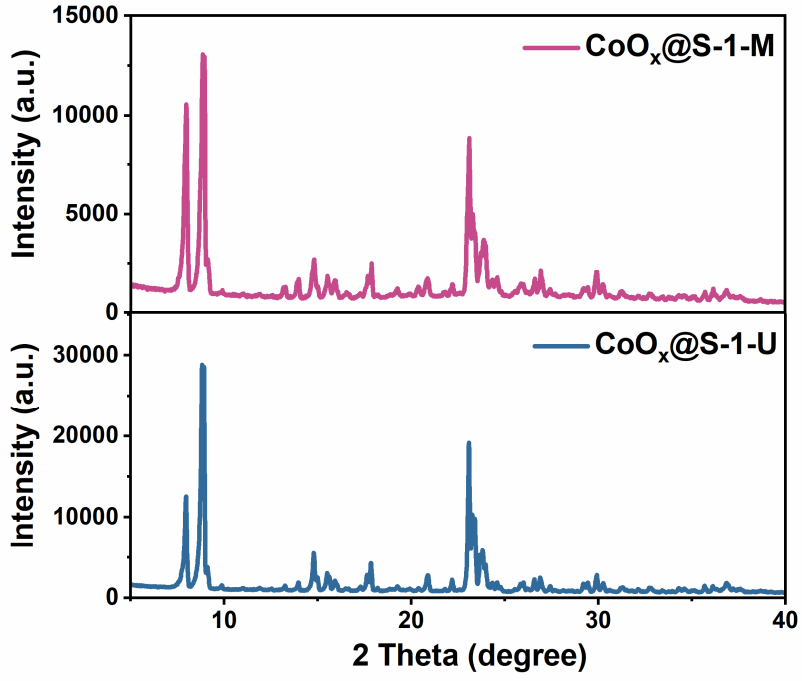

Figure S2. The X-ray diffraction patterns of CoO_x@S-1-M and CoO_x@S-1-U demonstrate the structural properties of both catalysts.

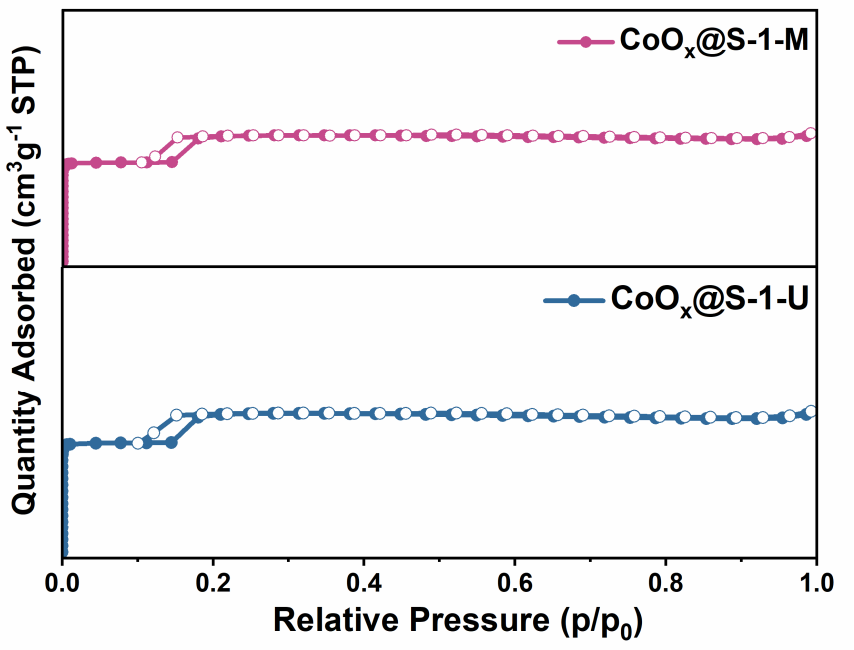

Figure S3. Nitrogen adsorption-desorption isotherms confirm the presence of a well-developed microporous structure in both CoO_x@S-1-M and CoO_x@S-1-U.

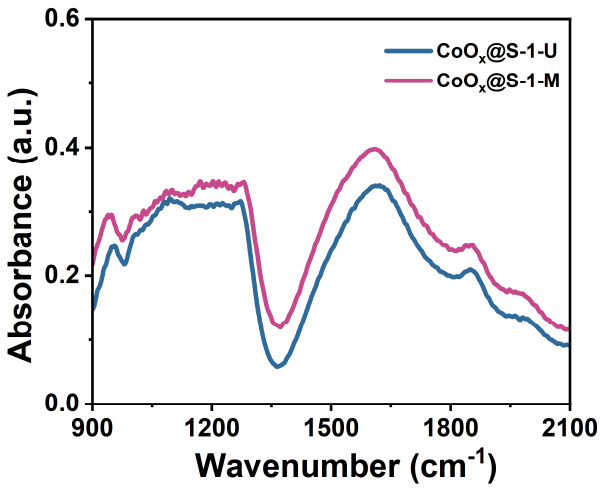

Figure S4. Infrared absorption spectra of CoO_x@S-1-M and CoO_x@S-1-U. A prominent band near 1090 cm^{-1} is attributed to the vibrations of Si-O-Si bridges. Additionally, the appearance of a band around 1000 cm^{-1}, assigned to Co-O-Si vibrations, indicates the incorporation of cobalt species into the zeolite framework.

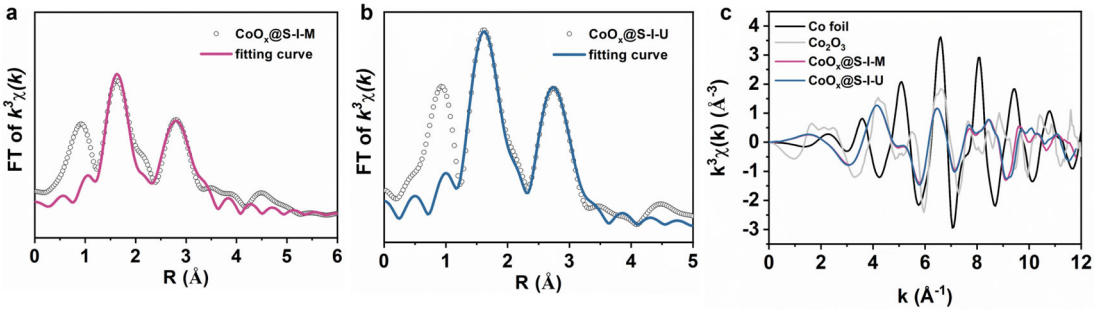

Figure S5. (a) CoO_x@S-1-M and (b) CoO_x@S-1-U K-edge EXAFS (circle) and fitting curve (line), shown in R-space. (c) Co K-edge EXAFS spectra of Co foil, Co_2O_3, CoO_x@S-1-M and CoO_x@S-1-U, shown in k^3- weighted *k*-space.

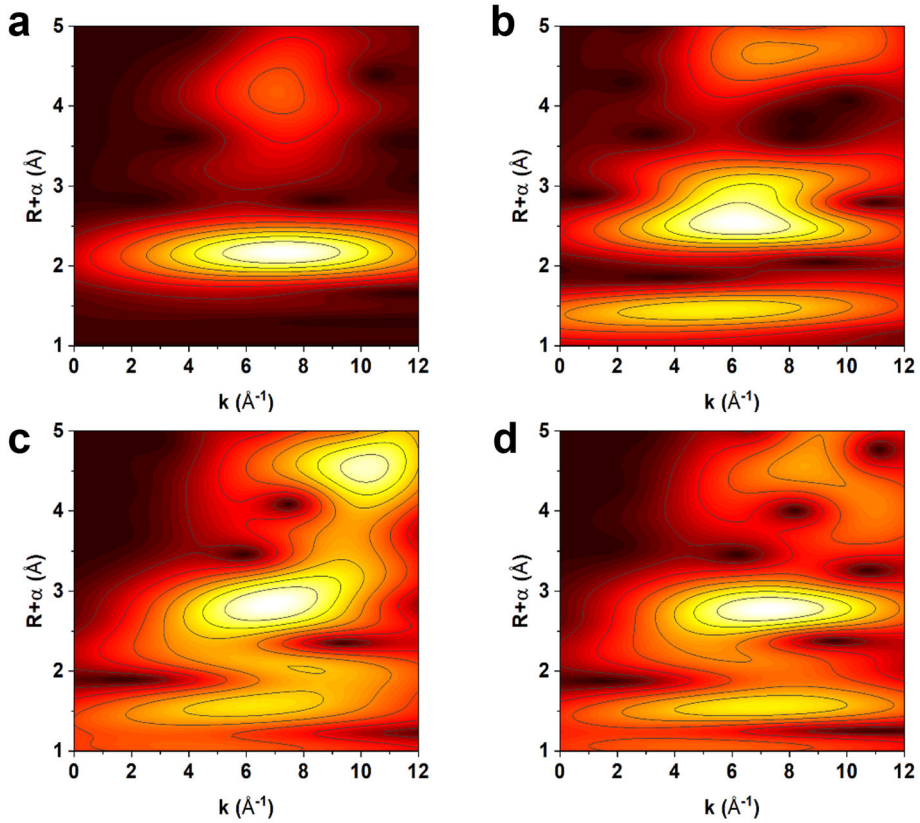

Figure S6. Wavelet transform analysis was performed on (a)-(d), corresponding to Co, Co_2O_3, CoO_x@S-1-M, and CoO_x@S-1-U, respectively. The results confirm that the CoO_x species within the molecular sieve channels exist as clusters rather than isolated Co species.

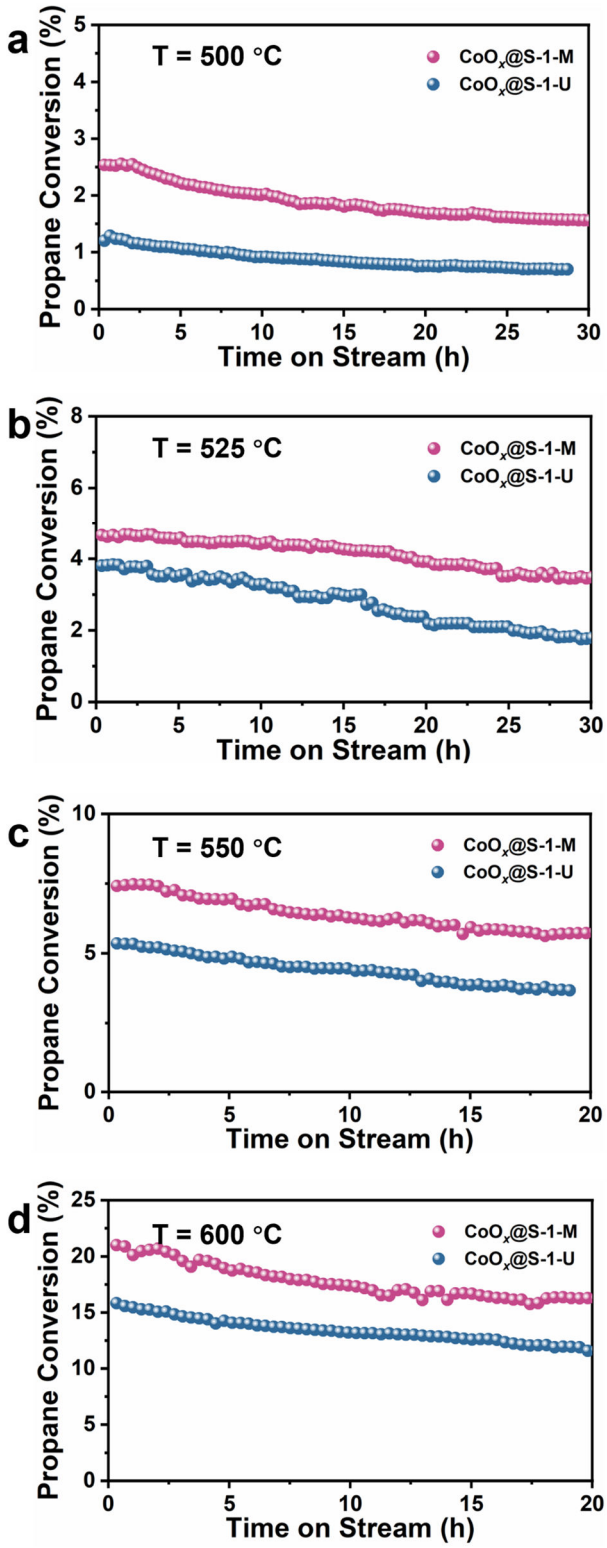

Figure S7. Durability of CoO_x@S-1-M and CoO_x@S-1-U catalysts. Reaction conditions: feed gas of 20% C_3H_8 and 80% N_2, WHSV = 2.16 $g_{C3H8} \cdot g_{zeo.}^{-1} \cdot h^{-1}$.

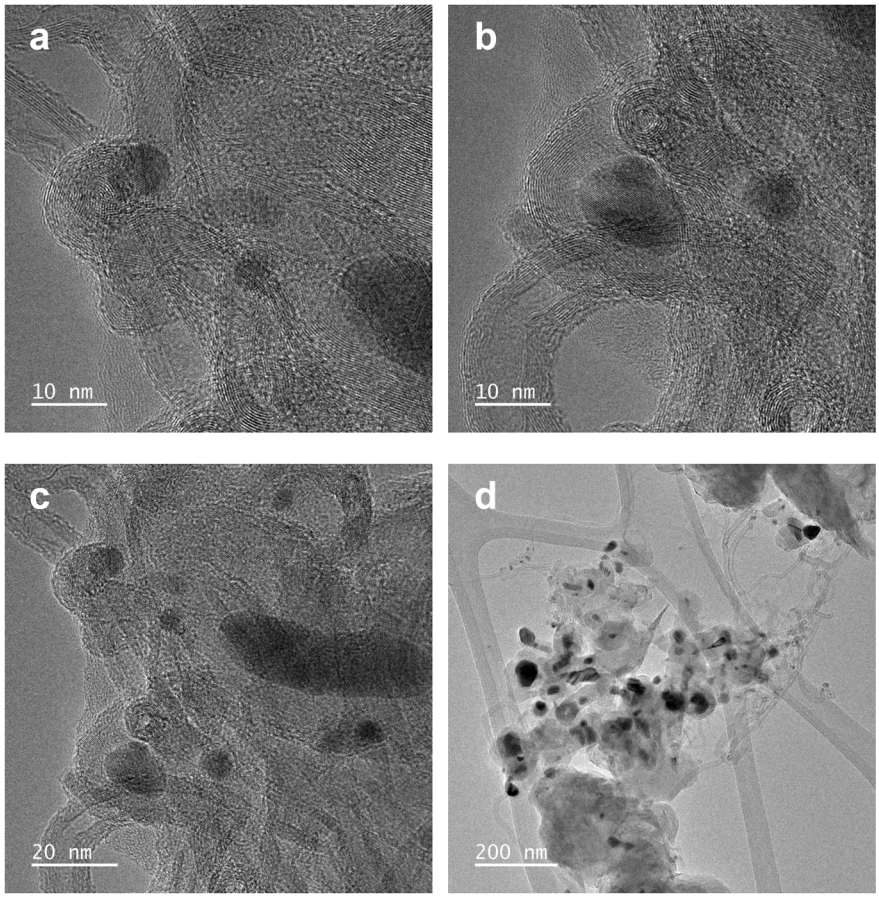

Figure S8. STEM image of the deactivated CoO_x/SiO_2 catalyst.

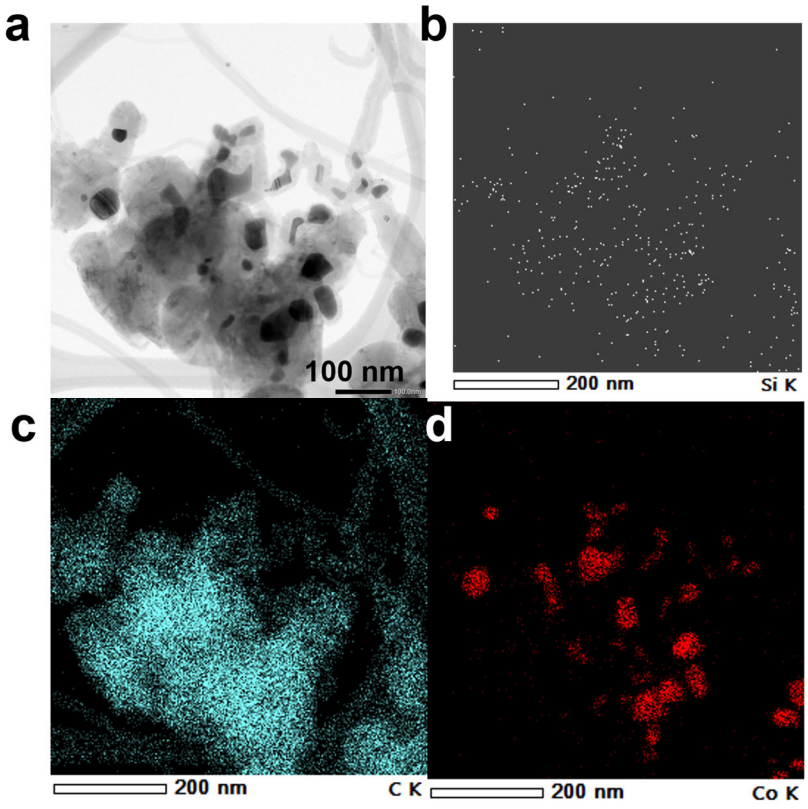

Figure S9. STEM-EDS elemental mapping images of the deactivated CoO_x/SiO_2 catalyst: Si (white), C (blue), and Co (red). A large amount of carbon deposition and Co species aggregated into large particles from smaller clusters can be clearly observed.

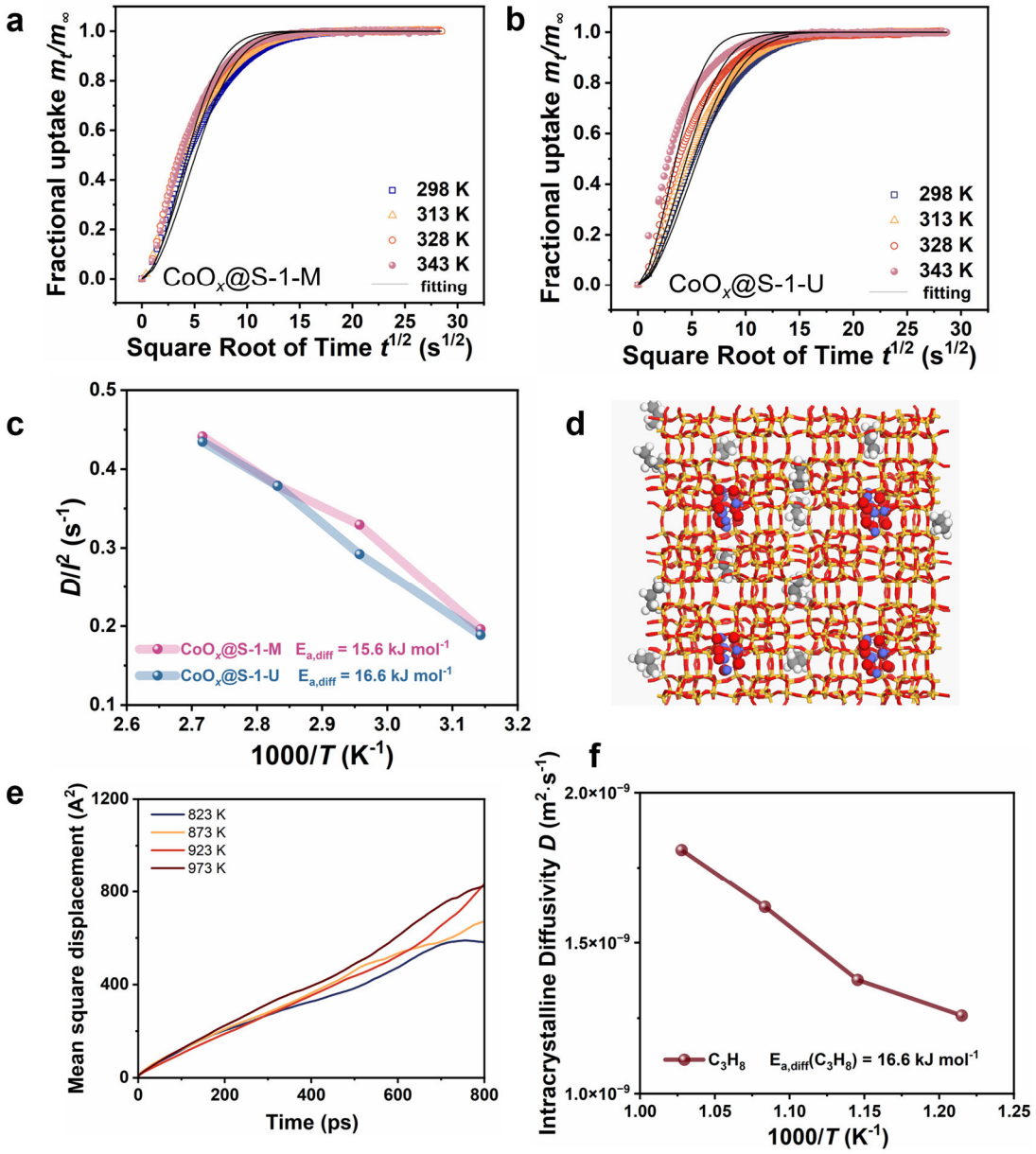

Figure S10. The uptake curves of propane in (a) CoO_x@S-1-M and (b) CoO_x@S-1-U at 25, 40, 55 and 70 °C (0 → 10 mbar), respectively (details are summarized in Table S3). (c) The inverse of diffusion time constant of propane in CoO_x@S-1-M and CoO_x@S-1-U respectively. (d) The structure used for MD simulations. Orange, red, and violet spheres represent Si, O, and Co atoms, respectively. (e) The mean square displacement of C_3H_8 at 823, 873, 923 and 973 K, respectively. (f) The self-diffusivities of C_3H_8 at 823, 873, 923 and 973 K, respectively.

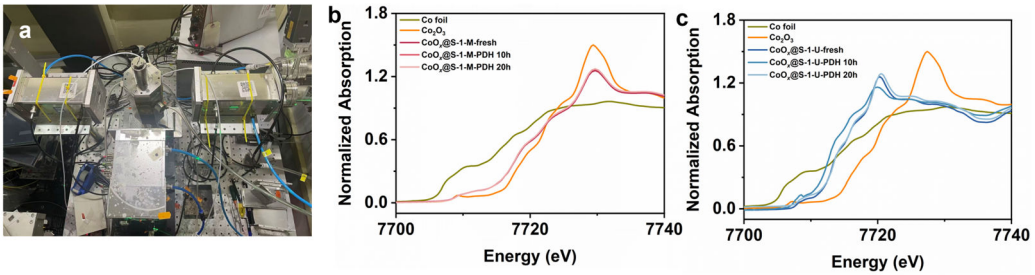

Figure S11. (a) Schematic diagram of the *in situ* XAFS setup used for monitoring the structural evolution of Co species during the PDH reaction. k-edge XANES spectra of (b) CoO_x@S-1-M and (c) CoO_x@S-1-U catalysts at different times on stream compared with reference spectra of Co foil and Co_2O_3. Reaction conditions: feed gas of 20% C_3H_8 and 80% N_2, WHSV = 2.16 $g_{C3H8} \cdot g_{zeo.}^{-1} \cdot h^{-1}$, set temperature of *in situ* cell T = 575 °C.

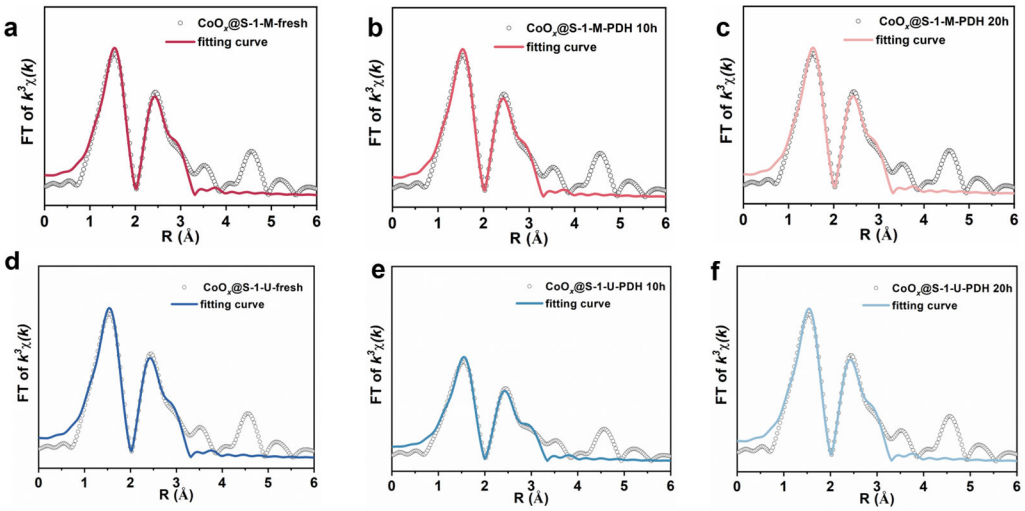

Figure S12. CoO_x@S-1-M and CoO_x@S-1-U at different times on stream K-edge EXAFS (circle) and fitting curve (line), shown in R-space.

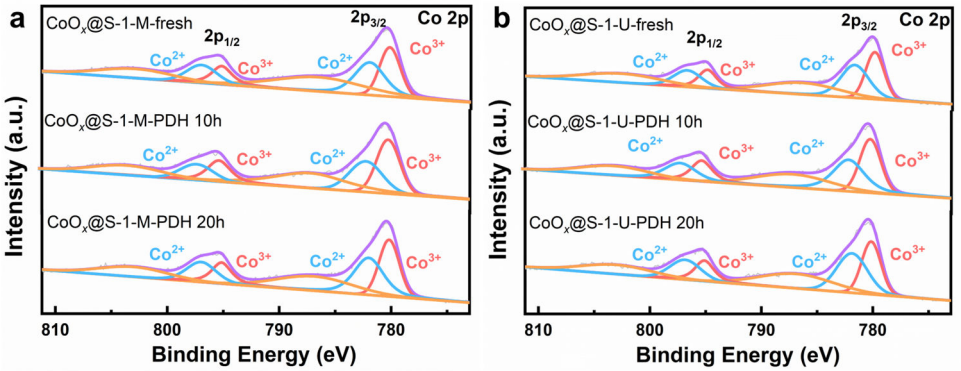

Figure S13. XPS spectra of (a) CoO_x@S-1-M and (b) CoO_x@S-1-U on different times on stream. The catalysts were collected after 10 h and 20 h of reaction in a fixed-bed reactor under conditions of a feed gas containing 20% C_3H_8 and 80% N_2, WHSV = 2.16 $g_{C3H8}\cdot g_{zeo.}^{-1}\cdot h^{-1}$ and a set temperature of 575 °C.

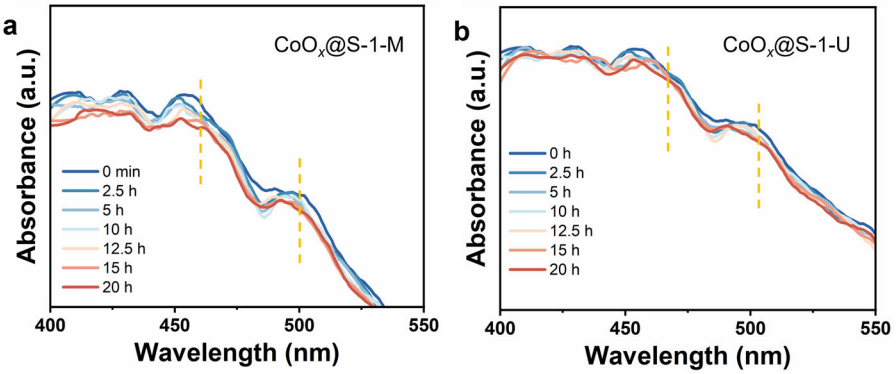

Figure S14. *In situ* UV-vis spectra of (a) CoO_x@S-1-M and (b) CoO_x@S-1-U during PDH. Reaction conditions: feed gas of 20% C_3H_8 and 80% N_2, WHSV = 2.16 $g_{C3H8}\cdot g_{zeo.}^{-1}\cdot h^{-1}$, set temperature of *in situ* cell T = 575 °C.

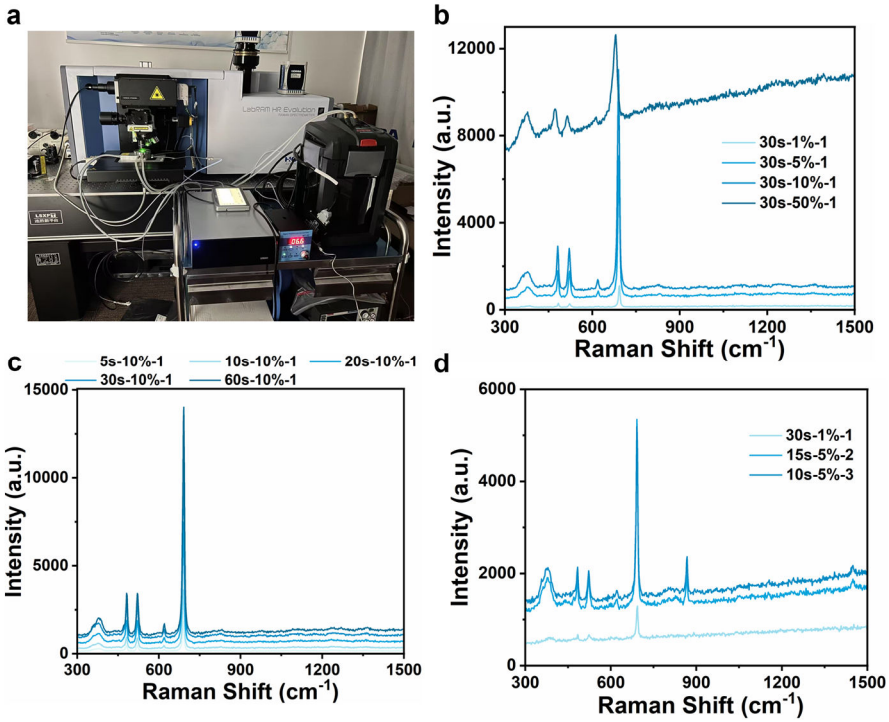

Figure S15. (a) High-speed high-resolution confocal Raman spectrometer. (b)-(d) Raman spectra were obtained under different laser power conditions, varying exposure times and different cycle numbers. However, we observed that 50% power increased the local temperature. To avoid thermal effects during testing, we selected parameters of 10% exposure power, a single cycle, and exposure times of 20 s.

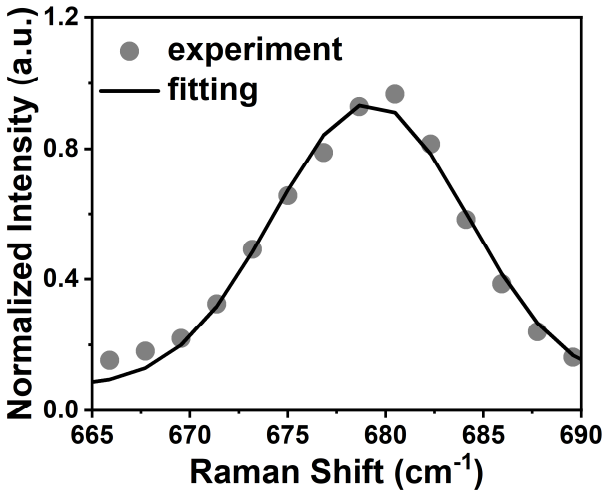

Figure S16. The Raman spectrum of the Co-O Raman peak of CoO_x@S-1-M and its corresponding fitting curve.

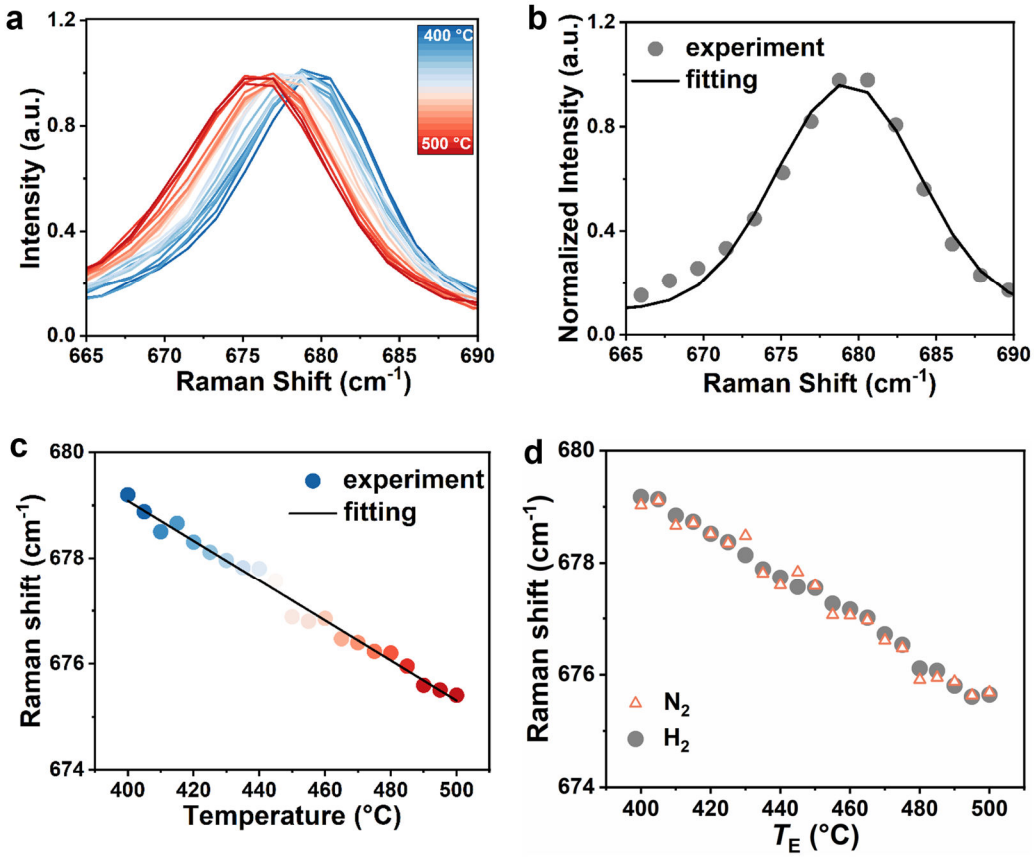

Figure S17. (a) Temperature-dependent Raman shift of the Co-O characteristic peak in CoO_x@S-1-U; (b) Raman spectrum of the Co-O vibration in CoO_x@S-1-U along with its fitted curve; (c) Linear correlation between the Co-O Raman shift of CoO_x@S-1-U and temperature; (d) Comparison of the Raman shift of the fresh catalyst under N_2 (circle point) and 3%H_2/97%N_2 (triangle point) atmospheres.

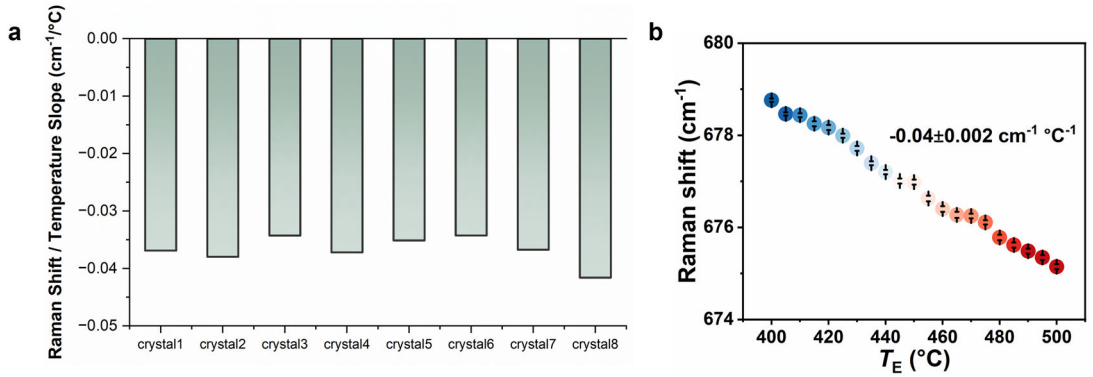

Figure S18. (a) Temperature-dependent Co-O Raman shifts of multiple crystals of CoO_x@S-1-M and CoO_x@S-1-U, respectively, showing consistent slopes of approximately -0.04 cm^{-1} $°C^{-1}$; (b) Mean and standard deviation of the characteristic peak positions across multiple crystals at each temperature, together with the slope of the Raman shift–temperature relation and its standard deviation.

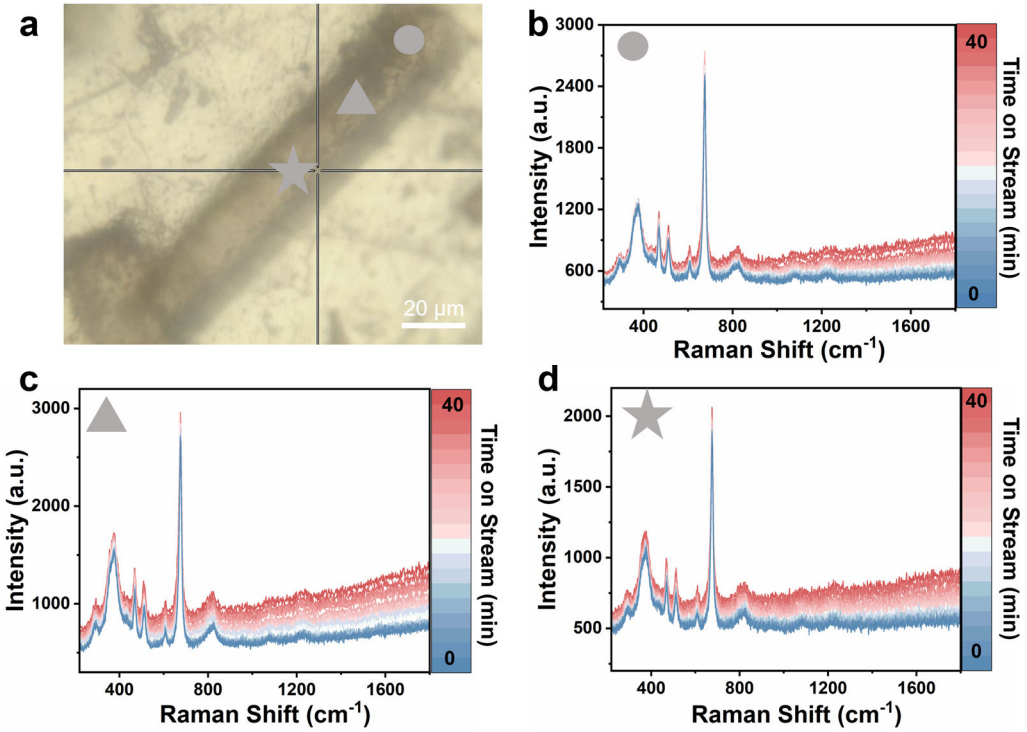

Figure S19. Time-resolved Raman spectra of different regions within an individual CoO_x@S-1-U crystal during the PDH reaction.

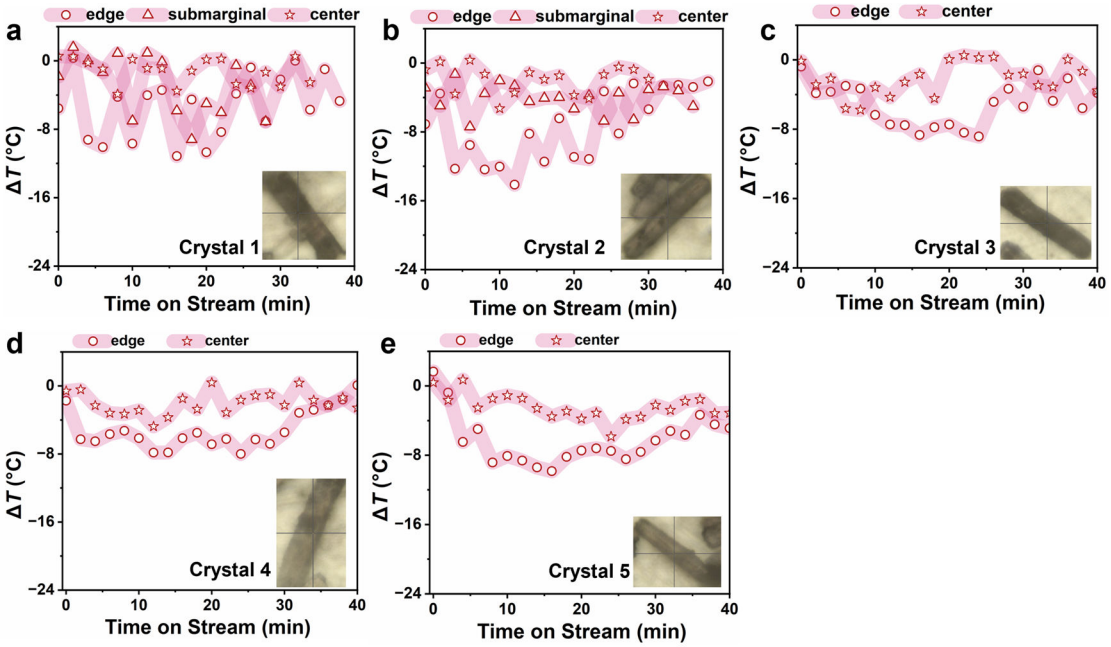

Figure S20. Temporal evolution of the temperature of active CoO_x clusters in different regions of CoO_x@S-1-M crystals during the PDH reaction. Reaction conditions: feed gas of 20% C_3H_8 and 80% N_2, flow rate F = 5ml/min, set temperature of *in situ* cell T = 575 °C. Raman excitation wavelength: 532 nm, with a 20 s exposure time and a single cycle for each spectrum.

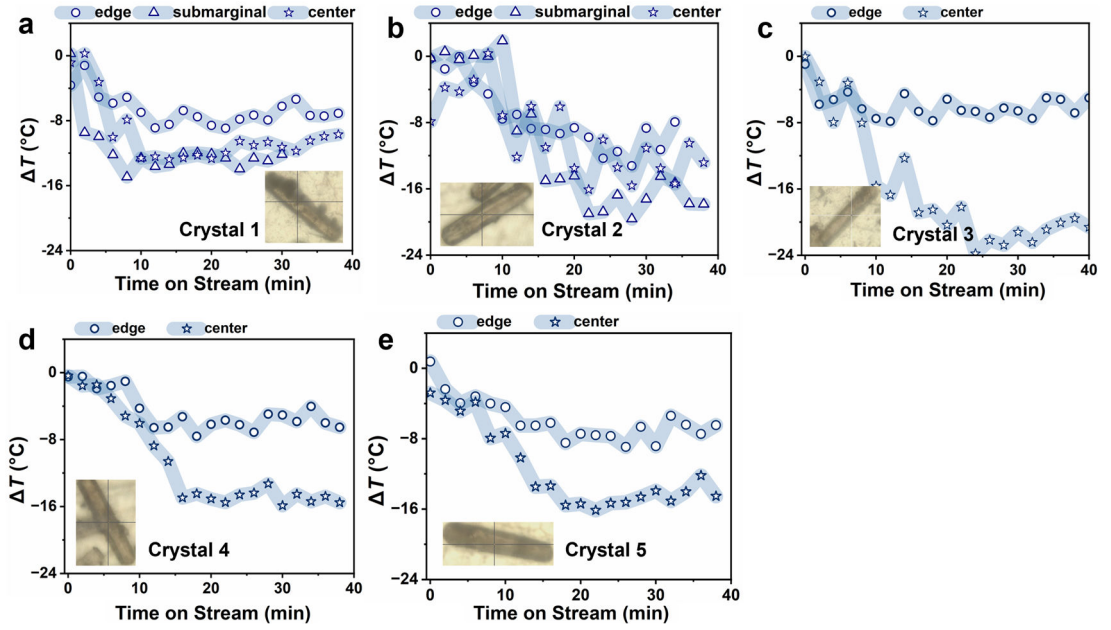

Figure S21. Temporal evolution of the temperature of active CoO_x clusters in different regions of CoO_x@S-1-U crystals during the PDH reaction. Reaction conditions: feed gas of 20% C_3H_8 and 80% N_2, flow rate F = 5ml/min, set temperature of *in situ* cell T = 575 °C. Raman excitation wavelength: 532 nm, with a 20 s exposure time and a single cycle for each spectrum

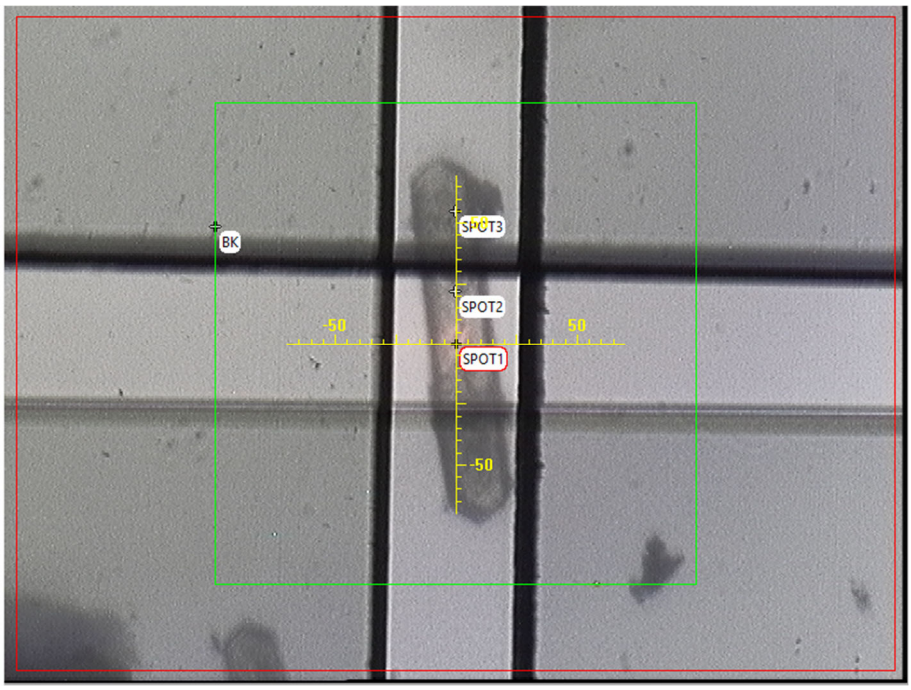

Figure S22. Bright-field images of the CoO_x-S-1 obtained using IR.

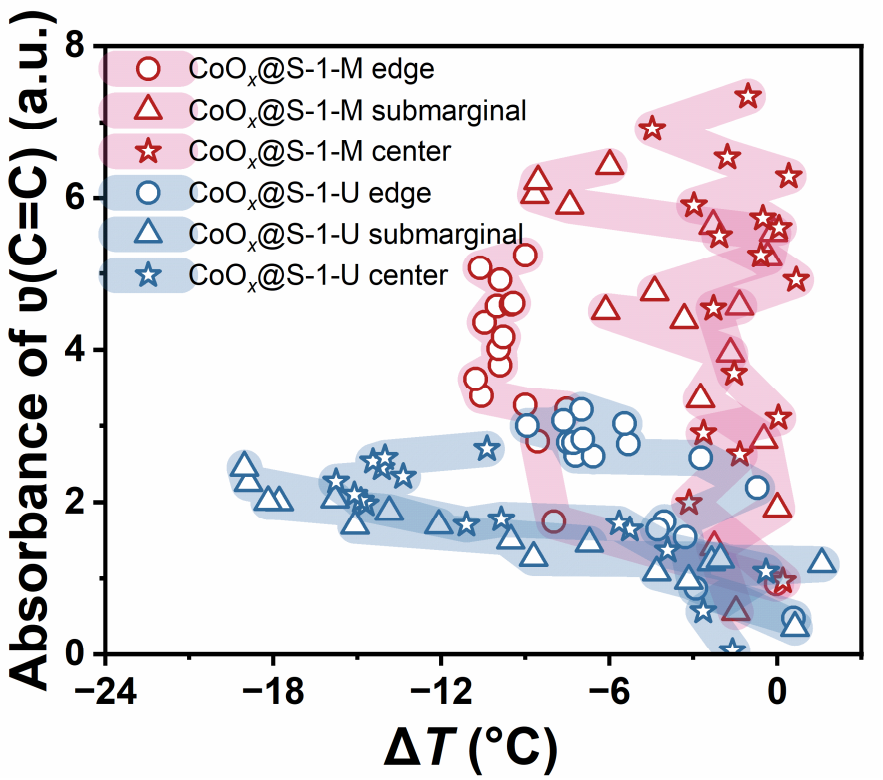

Figure S23. Relationship between local temperature and local intermediate formation within an individual crystal.

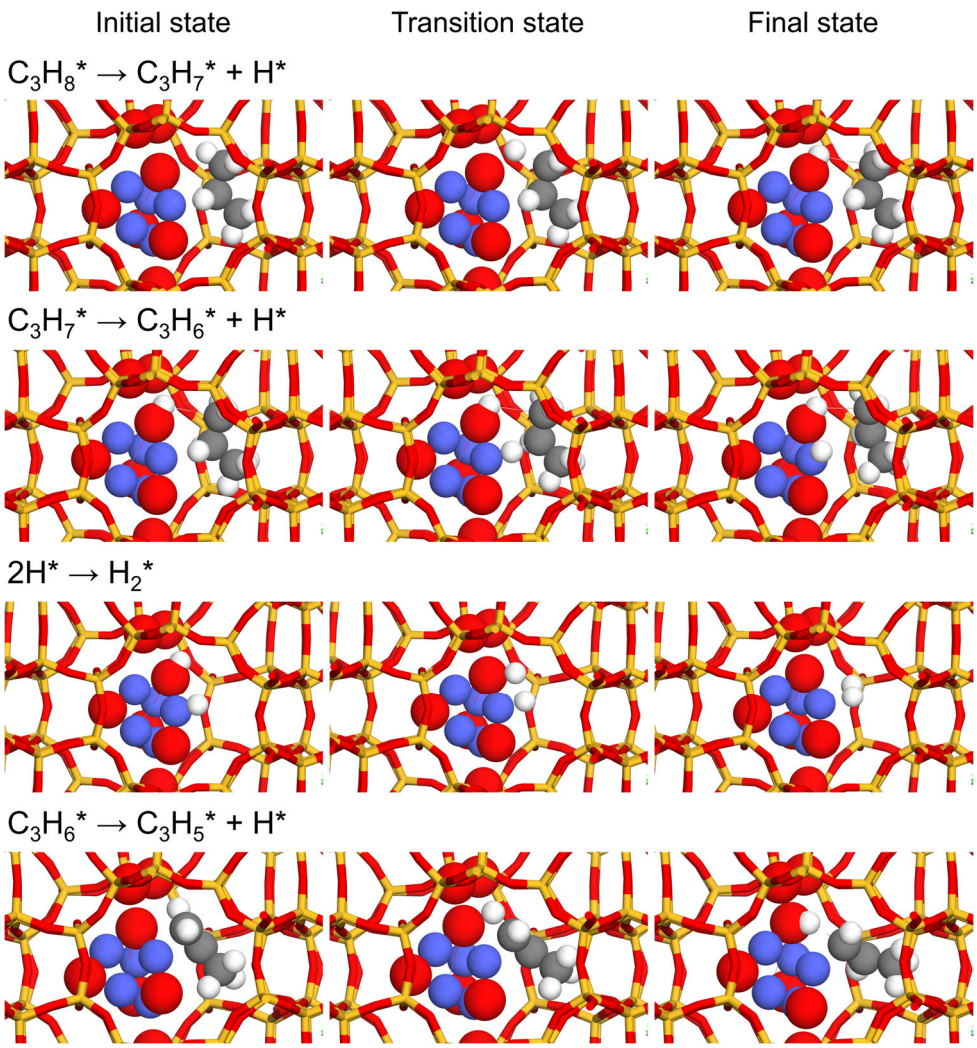

Figure S24. Geometries of initial (IS) transitional (TS) and final (FS) states for the dehydrogenation of propane, propyl isomer, H_2 and propylene formation over active CoO_x clusters within S-1. Orange, red, and violet spheres represent Si, O, and Co atoms, respectively, while dark gray and white spheres denote C and H atoms.

3. Supplemental Tables

Table S1. Co species concentration, BET surface area and micropore volume of CoO_x@S-1-M and CoO_x@S-1-U.

	CoO_x@S-1-M	CoO_x@S-1-U
metal content (%)	5.4	5.1
S_{BET} (m^2g^{-1})	345.9	349.1
maximum pore volume (cm^3/g)	0.13	0.13

BET surface area and average pore diameter are determined from multipoint method. Maximum pore volume is determined from the Horvath-Kawazoe method at P/P_0 = 0.08.

Table S2. EXAFS fitting parameters at the Co K-edge of CoO_x@S-1-M and CoO_x@S-1-U (S_0^2=0.92).

samples	path	C. N.[a]	R (Å) [b]	σ^2 ($\times 10^{-3}$ Å^2) [c]	ΔE (eV) [d]	R factor[e]
CoO_x@S-1-M	Co-O	4.9	2.05	5.3	7.8	0.02
	Co-O-Co	4.0	3.15	3.2		
	Co-O-Si	2.4	3.35	5.0		
CoO_x@S-1-U	Co-O	5.2	2.04	2.2	6.8	0.02
	Co-O-Co	4.2	3.11	7.8		
	Co-O-Si	3.6	3.32	2.3		

[a]C. N.: coordination numbers; [b]*R*: bond distance; [c]σ^2: Debye-Waller factors; [d]ΔE_0: the inner potential correction. [e]*R* factor: goodness of fit.

Table S3. Equilibrium conversions of propane in PDH over CoO_x@S-1-M and CoO_x@S-1-U at different temperatures.

Temperature (K)	Equilibrium Conversion %
773	33.6
798	43.0
823	53.0
848	62.8
873	71.8

Table S4. Parameters of propane diffusion in S-1 channels.

Temperature (K)	CoO_x@S-1-M			CoO_x@S-1-U		
	D/l^2 (s^{-1})	α/l (mol/(m^3·s·Pa))	R^2	D/l^2 (s^{-1})	α/l (mol/(m^3·s·Pa))	R^2
293	1.78	0.51	0.97	1.18	0.57	0.98
313	2.06	0.65	0.96	1.83	0.47	0.98
328	2.93	0.61	0.96	2.37	0.62	0.95
343	3.59	0.57	0.97	4.94	0.86	0.93

Table S5. Parameters used for assessing external and internal mass transfer limitations over CoO_x@S-1-M and CoO_x@S-1-U in PDH reactions.

Parameters	CoO_x@S-1-M	CoO_x@S-1-U
Catalyst mass, $g_{cat.}$	0.05	0.05
Weight hourly space velocity, WHSV, h^{-1}	2.16	2.16
Reaction temperature T, °C	600 °C	600 °C
Reaction pressure p, MPa	0.10	0.10
Solid catalyst density ρ_c, $kg \cdot m^{-3}$	2200	2200
Catalyst bed density ρ_b, $kg \cdot m^{-3}$	7.70×10^{2}	7.70×10^{2}
Catalyst particle radius R_{cat}, m	6.00×10^{-6}	6.00×10^{-6}
Reaction rate $-r_A$, $kmol \cdot kg^{-1} \cdot s^{-1}$	2.71×10^{-6}	2.17×10^{-6}
Reaction order n	1.00	1.00
Mass transfer coefficient k_c, $m \cdot s^{-1}$	7.53	7.53
Bulk gas concentration of propane C_{Ab}, $kmol \cdot m^{-3}$	1.40×10^{-2}	1.40×10^{-2}
Gas phase diffusivity of propane D_{gas}, $m^2 \cdot s^{-1}$	4.38×10^{-5}	4.38×10^{-5}
Intracrystalline diffusivity of propane in MFI D_{intra}, $m^2 \cdot s^{-1}$	1.38×10^{-9}	1.38×10^{-9}
Mears' criterion (external mass transfer)	$1.19\times10^{-7} << 0.15$	$9.55\times10^{-8} << 0.15$
Weisz-Prater' criterion (internal mass transfer)	$0.011 << 1$	$0.0090 << 1$

Notes: As can be seen from Table S5, external and internal mass transfer effects can be negligible under the reaction conditions.

(1) Details for (CoO_x@S-1-M, T = 873 K, P = 0.1 MPa, WHSV = 2.16 h^{-1})

[a] Reaction rate $-r_A$,

$-r_A = \frac{F_{C_3H_8} \times X_{C_3H_8}}{M_{cat.}}$ (where $F_{C_3H_8}$ is the flow rate of C_3H_8 in $mol \cdot s^{-1}$, $X_{C_3H_8}$ is the conversion of propane, $M_{cat.}$ is the weight of the catalyst in g;

$-r_A = \frac{F_{C_3H_8} \times X_{C_3H_8}}{M_{cat.}} = 2.71\times10^{-6}$ $kmol \cdot kg^{-1} \cdot s^{-1}$;

[b] Solid catalyst density ρ_c

ρ_c=2200 $kg \cdot m^{-3}$ is obtained from experiment;

[c] Catalyst bed density ρ_b, $\rho_b = (1 - \emptyset) \cdot \rho_c$, $\emptyset$=0.65 is obtained from experiment;

ρ_b=2200 $kg \cdot m^{-3}$ × (1-0.65) = 7.70×10^{2} $kg \cdot m^{-3}$

[d] Catalyst particle radius R_{cat}, i.e. the length of b-axis of S-1, $R_{cat}=\frac{1}{2}L_b=6.00\times10^{-6}$ m;

[e] Reaction order n, n = 1 is obtained from experiments;

[f] Mass transfer coefficient k_c

Sherwood number (Sh) = $k_c\cdot(2R_{cat})/D_{gas}$

$Sh = 2 + 0.6Re^{1/2}\cdot Sc^{1/3}$;

Reynolds number (Re) = $2U\cdot R\cdot\rho/\mu$ (where U is superficial velocity in $m\cdot s^{-1}$, $U_{298K}=1.15\times10^{-2}$ $m\cdot s^{-1}$, $U_{873K}=3.37\times10^{-2}$ $m\cdot s^{-1}$, ρ is the density of the propane in $kg\cdot m^{-3}$, $\rho_{298K}=$ 1.81 $kg\cdot m^{-3}$, $\rho_{873K}=$ 0.62 $kg\cdot m^{-3}$, μ is the viscosity of the propane in Pa·s, $\mu_{298K}=$ 8.12×10^{-6} Pa·s, $\mu_{873K}=$ 1.39×10^{-5} Pa·s);

$$Re = 2U\cdot R\cdot\rho/\mu=\frac{2\times3.37\times10^{-2}\ m\cdot s^{-1}\times6.00\times10^{-6}\ m\times0.62\ kg\cdot m^{-3}}{1.39\times10^{-5}\ Pa\cdot s}=0.018$$

$D_{gas}=\frac{0.00266\cdot T^{1.5}\cdot(\frac{1}{M_A})^{0.5}}{\sigma_{AA}^2\cdot\Omega_{AA}}$ (where D_{gas} is gas-phase diffusivity in $m^2\cdot s^{-1}$, T is temperature in K, M_A is the molecular mass of propane in $g\cdot mol^{-1}$, Ω_{AA} is collision integral of propane, σ_{AA} is constant of Lennard-Jones potential energy function.)

$$D_{gas}=\frac{0.00266\cdot T^{1.5}\cdot(\frac{1}{M_A})^{0.5}}{\sigma_{AA}^2\cdot\Omega_{AA}}=\frac{0.00266\times(873\ K)^{1.5}\times(\frac{1}{44\ g\cdot mol^{-1}})^{0.5}}{5.118^2\times0.902}=4.38\times10^{-5}\ m^2\cdot s^{-1}$$

Schmidt number (Sc) = $\mu/(\rho\cdot D_{gas})$;

$$Sc = \mu/(\rho\cdot D_{gas})=\frac{1.39\times10^{-5}\ Pa\cdot s}{0.62\ kg\cdot m^{-3}\times4.38\times10^{-5}\ m^2\cdot s^{-1}}=5.12\times10^{-1}$$

$$k_c=\frac{Sh\cdot D_{gas}}{2R_{cat}}=\frac{\left(2+0.6\times Re^{\frac{1}{2}}\cdot Sc^{\frac{1}{3}}\right)\cdot D_{gas}}{2R_{cat}}=\frac{\left(2+0.6\times(0.018)^{\frac{1}{2}}\times\left(5.12\times10^{-1}\right)^{\frac{1}{3}}\right)\times4.38\times10^{-5}\ m^2\cdot s^{-1}}{2\times6.00\times10^{-6}\ m}$$

$=7.53\ m\cdot s^{-1}$

[g] Bulk gas concentration of propane at T=600 °C (873K) C_{Ab},

$C_{Ab}=\frac{P}{RT}$ (where p is the pressure in kPa, T is temperature in K, R is the gas constant in $J\cdot(K\cdot mol)^{-1}$.)

$$C_{Ab}=\frac{P}{RT}=\frac{101.325\ kPa}{8.314\ J\cdot(K\cdot mol)^{-1}\times873\ K}=1.40\times10^{-2}\ kmol\cdot m^{-3}$$

[h] Intracrystalline diffusivity of propane at 873 K in S-1, D_{intra}

D_{intra}=1.38×10^{-9} m^2·s^{-1} is obtained from molecular dynamics (sees detailed method for calculation in page X of supporting information and **Supplementary Fig. S7**).

Weisz-Prater' criterion:

$$C_{WP} = \frac{-r_A \rho_c R_{cat}^2}{D_{intra} C_{Ab}} = \frac{2.71\times10^{-6}\ \text{kmol·kg}^{-1}\text{·s}^{-1}\times2.20\times10^{3}\ \text{kg·m}^{-3}\times(6.00\times10^{-6}\ \text{m})^2}{1.38\times10^{-9}\ \text{m}^2\text{·s}^{-1}\times1.40\times10^{-2}\ \text{kmol·m}^{-3}} = 0.011 < 1$$

Mears' criterion:

$$C_M = \frac{-r_A \rho_b R_{cat} n}{k_c C_{Ab}} = \frac{2.71\times10^{-6}\ \text{kmol·kg}^{-1}\text{·s}^{-1}\times7.70\times10^{2}\ \text{kg·m}^{-3}\times6.00\times10^{-6}\ \text{m}\times1}{7.53\ \text{m·s}^{-1}\times1.40\times10^{-2}\ \text{kmol·m}^{-3}} = 1.19\times10^{-7} < 0.15$$

(2) Details for (CoO_x@S-1-U, T = 873 K, P = 0.1 MPa, WHSV = 2.16 h^{-1})

[a] Reaction rate -r_A,

$-r_A = \frac{F_{C_3H_8}\times X_{C_3H_8}}{M_{cat.}}$ (where $F_{C_3H_8}$ is the flow rate of C_3H_8 in mol·s^{-1}, $X_{C_3H_8}$ is the conversion of propane, $M_{cat.}$ is the weight of the catalyst in g;

$-r_A = \frac{F_{C_3H_8}\times X_{C_3H_8}}{M_{cat.}}$ = 2.17×10^{-6} kmol·kg^{-1}·s^{-1};

[b] Solid catalyst density ρ_c

ρ_c=2200 kg·m^{-3} is obtained from experiment;

[c] Catalyst bed density ρ_b, $\rho_b = (1-\emptyset)\cdot\rho_c$, $\emptyset$=0.65 is obtained from experiment;

ρ_b=2200 kg·m^{-3} × (1-0.65) = 7.70×10^2 kg·m^{-3}

[d] Catalyst particle radius R_{cat}, i.e. the length of b-axis of S-1, $R_{cat}=\frac{1}{2}L_b$=6.00×10^{-6} m;

[e] Reaction order n, n = 1 is obtained from experiments;

[f] Mass transfer coefficient k_c

Sherwood number (Sh) = k_c·(2R$_{cat}$)/D_{gas}

Sh = 2 + 0.6Re$^{1/2}$·Sc$^{1/3}$;

Reynolds number (Re) = $2U·R·\rho/\mu$ (where U is superficial velocity in m·s^{-1}, U_{298K}=1.15×10^{-2} m·s^{-1}, U_{873K}=3.37×10^{-2} m·s^{-1}, ρ is the density of the propane in kg·m^{-3}, ρ_{298K}= 1.81 kg·m^{-3}, ρ_{873K}= 0.62 kg·m^{-3}, μ is the viscosity of the propane in Pa·s, μ_{298K}= 8.12×10^{-6} Pa·s, μ_{873K}= 1.39×10^{-5} Pa·s);

$\mathrm{Re} = 2U{\cdot}R{\cdot}\rho/\mu = \frac{2\times3.37\times10^{-2}\ \mathrm{m{\cdot}s^{-1}}\times6.00\times10^{-6}\ \mathrm{m}\times0.62\ \mathrm{kg{\cdot}m^{-3}}}{1.39\times10^{-5}\ \mathrm{Pa{\cdot}}s} = 0.018$

$D_{\mathrm{gas}} = \frac{0.00266{\cdot}T^{1.5}{\cdot}(\frac{1}{M_A})^{0.5}}{\sigma_{AA}^2{\cdot}\Omega_{AA}}$ (where D_{gas} is gas-phase diffusivity in $\mathrm{m^2{\cdot}s^{-1}}$, T is temperature in K, M_{A} is the molecular mass of propane in $\mathrm{g{\cdot}mol^{-1}}$, Ω_{AA} is collision integral of propane, σ_{AA} is constant of Lennard-Jones potential energy function.)

$D_{\mathrm{gas}} = \frac{0.00266{\cdot}T^{1.5}{\cdot}(\frac{1}{M_A})^{0.5}}{\sigma_{AA}^2{\cdot}\Omega_{AA}} = \frac{0.00266\times(873\ \mathrm{K})^{1.5}\times(\frac{1}{44\ \mathrm{g{\cdot}mol^{-1}}})^{0.5}}{5.118^2\times0.902} = 4.38\times10^{-5}\ \mathrm{m^2{\cdot}s^{-1}}$

Schmidt number (Sc) = $\mu/(\rho{\cdot}D_{\mathrm{gas}})$;

$\mathrm{Sc} = \mu/(\rho{\cdot}D_{\mathrm{gas}}) = \frac{1.39\times10^{-5}\ \mathrm{Pa{\cdot}}s}{0.62\ \mathrm{kg{\cdot}m^{-3}}\times4.38\times10^{-5}\ \mathrm{m^2{\cdot}s^{-1}}} = 5.12\times10^{-1}$

$k_c = \frac{Sh{\cdot}D_{\mathrm{gas}}}{2R_{cat}} = \frac{\left(2+0.6\times Re^{\frac{1}{2}}{\cdot}Sc^{\frac{1}{3}}\right){\cdot}D_{\mathrm{gas}}}{2R_{cat}} = \frac{\left(2+0.6\times(0.018)^{\frac{1}{2}}\times\left(5.12\times10^{-1}\right)^{\frac{1}{3}}\right)\times4.38\times10^{-5}\ \mathrm{m^2{\cdot}s^{-1}}}{2\times6.00\times10^{-6}\ \mathrm{m}}$

$=7.53\ \mathrm{m{\cdot}s^{-1}}$

[g] Bulk gas concentration of propane at T=600 °C (873K) C_{Ab},

$C_{Ab} = \frac{P}{RT}$ (where p is the pressure in kPa, T is temperature in K, R is the gas constant in $\mathrm{J{\cdot}(K{\cdot}mol)^{-1}}$.)

$C_{Ab} = \frac{P}{RT} = \frac{101.325\ \mathrm{kPa}}{8.314\ \mathrm{J{\cdot}(K{\cdot}mol)^{-1}}\times873\ \mathrm{K}} = 1.40\times10^{-2}\ \mathrm{kmol{\cdot}m^{-3}}$

[h] Intracrystalline diffusivity of propane at 873 K in S-1, D_{intra}

$D_{\mathrm{intra}}=1.38\times10^{-9}\ \mathrm{m^2{\cdot}s^{-1}}$ is obtained from molecular dynamics (sees detailed method for calculation in page X of supporting information and **Supplementary Fig. S7**).

Weisz-Prater' criterion:

$C_{WP} = \frac{-r_{\mathrm{A}}\rho_{\mathrm{c}}R_{\mathrm{cat}}^2}{D_{\mathrm{intra}}C_{\mathrm{Ab}}} = \frac{2.17\times10^{-6}\ \mathrm{kmol{\cdot}kg^{-1}{\cdot}s^{-1}}\times2.20\times10^{3}\ \mathrm{kg{\cdot}m^{-3}}\times(6.00\times10^{-6}\ \mathrm{m})^2}{1.38\times10^{-9}\ \mathrm{m^2{\cdot}s^{-1}}\times1.40\times10^{-2}\ \mathrm{kmol{\cdot}m^{-3}}} = 0.0090 < 1$

Mears' criterion:

$C_M = \frac{-r_{\mathrm{A}}\rho_{\mathrm{b}}R_{\mathrm{cat}}n}{k_{\mathrm{c}}C_{\mathrm{Ab}}} = \frac{2.17\times10^{-6}\ \mathrm{kmol{\cdot}kg^{-1}{\cdot}s^{-1}}\times7.70\times10^{2}\ \mathrm{kg{\cdot}m^{-3}}\times6.00\times10^{-6}\ \mathrm{m}\times1}{7.53\ \mathrm{m{\cdot}s^{-1}}\times1.40\times10^{-2}\ \mathrm{kmol{\cdot}m^{-3}}} = 9.55\times10^{-8} <$ 0.15

Table S6. Information for calculating the effectiveness factor η and the Thiele modulus Φ over CoO_x@S-1-M and CoO_x@S-1-U, respectively.

Catalysts	CoO_x@S-1-M	CoO_x@S-1-U
The distance from center to edge of S-1 zeolite along b-axis l, m	6.00×10^{-6}	6.00×10^{-6}
Reaction rate $-r_A$, kmol·kg^{-1}·s^{-1}	2.71×10^{-6}	2.17×10^{-6}
Reaction rate constant k, s^{-1}	0.15	0.12
Intracrystalline diffusivity of propane in MFI D_{intra}, m^2·s^{-1}	1.38×10^{-9}	1.38×10^{-9}
Thiele modulus Φ	6.26×10^{-2}	5.60×10^{-2}
Effectiveness factor η	0.999	0.999

[a] The distance from center to edge of S-1 zeolite along b-axis l, m

$l = L_b/2$ (L_b is length of b-axis of S-1 zeolite in m),

$l = 6.00\times10^{-6}$ m,

[b] Reaction rate $-r_A$, kmol·kg^{-1}·s^{-1}

$-r_A = \frac{F_{C_3H_8}\times X_{C_3H_8}}{M_{cat.}}$ (where $F_{C_3H_8}$ is the flow rate of C_3H_8 in mol·s^{-1}, $X_{C_3H_8}$ is the conversion of propane, $M_{cat.}$ is the weight of the catalyst in g;

$-r_{A(CoOx@S-1-M)} = \frac{F_{C_3H_8}\times X_{C_3H_8}}{M_{cat.}} = 2.71\times10^{-6}$ kmol·kg^{-1}·s^{-1};

$-r_{A(CoOx@S-1-U)} = \frac{F_{C_3H_8}\times X_{C_3H_8}}{M_{cat.}} = 2.17\times10^{-6}$ kmol·kg^{-1}·s^{-1};

[c] Reaction rate constant k, s^{-1}

$C_A = \frac{P}{RT}$ (where p is the pressure in kPa, T is temperature in K, R is the gas constant in J·(K·mol)$^{-1}$.)

$C_A = \frac{P}{RT} = \frac{101.325\ \text{kPa}}{8.314\ \text{J·(K·mol)}^{-1}\times873\ \text{K}} = 1.40\times10^{-2}$ kmol·m^{-3}

$k_{CoOx@S-1-M} = \frac{-r_A'}{C_A} = \frac{-r_A\rho_b}{C_A} = \frac{2.71\times10^{-6}\ \text{kmol·kg}^{-1}\text{·s}^{-1}\times7.70\times10^{2}\ \text{kg·m}^{-3}}{1.40\times10^{-2}\ \text{kmol·m}^{-3}} = 0.15$·s^{-1};

$k_{CoOx@S-1-U} = \frac{-r_A'}{C_A} = \frac{-r_A\rho_b}{C_A} = \frac{2.71\times10^{-6}\ \text{kmol·kg}^{-1}\text{·s}^{-1}\times7.70\times10^{2}\ \text{kg·m}^{-3}}{1.40\times10^{-2}\ \text{kmol·m}^{-3}} = 0.12$·s^{-1};

[d] Intracrystalline diffusivity of propane at 873 K in S-1, D_{intra}

$D_{intra} = 1.38\times10^{-9}$ m^2·s^{-1} is obtained from density functional theory computation;

[e] Thiele modulus Φ,

$\Phi = l(k/D_{\text{intra}})^{1/2}$

$\Phi_{\text{CoO}x@\text{S}-1-\text{M}} = l(k/D_{\text{intra}})^{1/2} = 6.26\times10^{-2}$;

$\Phi_{\text{CoO}x@\text{S}-1-\text{U}} = l(k/D_{\text{intra}})^{1/2} = 5.60\times10^{-2}$;

[f] Effectiveness factor η,

$\eta_{\text{CoO}x@\text{S}-1-\text{M}} = \frac{tan\Phi}{\Phi} = \frac{\tan(6.26\times10^{-2})}{6.26\times10^{-2}} = 0.999$;

$\eta_{\text{CoO}x@\text{S}-1-\text{U}} = \frac{tan\Phi}{\Phi} = \frac{\tan(5.60\times10^{-2})}{5.60\times10^{-2}} = 0.999$

Table S7. EXAFS fitting parameters at the Co K-edge of CoO_x@S-1-M and CoO_x@S-1-U at different times on stream. (S_0^2=0.73).

samples	path	C. N.[a]	R (Å) [b]	σ^2 ($\times 10^{-3}$ Å^2) [c]	ΔE (eV) [d]	R factor[e]
Co foil	Co-Co	12*	2.48	6.4	7.5	0.01
CoO_x@S-1-M-fresh	Co-O	5.1	2.00	7.7	0.4	0.02
	Co-O-Co	4.5	2.80	10.6		
	Co-O-Si	2.4	3.30	9.2		
CoO_x@S-1-M-PDH 10h	Co-O	5.2	2.00	7.8	0.4	0.02
	Co-O-Co	4.6	2.80	10.8		
	Co-O-Si	2.5	3.30	9.5		
CoO_x@S-1-M-PDH 20h	Co-O	5.2	2.00	7.9	0.3	0.02
	Co-O-Co	4.6	2.80	10.7		
	Co-O-Si	2.5	3.30	9.5		
CoO_x@S-1-U-fresh	Co-O	5.2	2.00	7.9	0.3	0.02
	Co-O-Co	4.6	2.80	10.8		
	Co-O-Si	2.5	3.30	9.7		
CoO_x@S-1-U-PDH 10h	Co-O	3.3	2.01	7.0	1.5	0.02
	Co-O-Co	3.1	2.82	10.6		
	Co-O-Si	1.3	3.32	6.7		
CoO_x@S-1-U-PDH 20h	Co-O	5.2	2.00	7.8	0.3	0.02
	Co-O-Co	4.6	2.80	10.8		
	Co-O-Si	2.5	3.30	9.6		

[a]C. N.: coordination numbers; [b]*R*: bond distance; [c]σ^2: Debye-Waller factors; [d]ΔE_0: the inner potential correction. [e]*R* factor: goodness of fit. *The experimental EXAFS fit by fixing C. N. as the known crystallographic value.

Table S8. Molecular composition of the extracts and the possible molecular structures.

Family	Formula	m/z range	Maximum peak
A	C_nH_{2n-10} $17 \leq n \leq 30$	229 - 411	397 ($C_{29}H_{48}$)
B	C_nH_{2n-26} $44 \leq n \leq 48$	591 - 648	648 ($C_{48}H_{70}$)
C	C_nH_{2n-64} $70 \leq n \leq 89$	917 - 1184	917 ($C_{70}H_{76}$)
D	C_nH_{2n-42} $99 \leq n \leq 110$	1346 - 1500	1374 ($C_{101}H_{160}$)